Am J Transl Res 2022;14(10):6924-6940
www.ajtr.org /ISSN:1943-8141/AJTR0143807

Original Article

Novel prognostic signature based on HRAS, MAPK3 and TFRC identified to be associated with ferroptosis and the immune microenvironment in hepatocellular carcinoma

Hanyao Sun[1], Xiyan Qian[2], Wei Yang[1], Weizhong Zhou[1], Chungao Zhou[1], Sheng Liu[1], Haibin Shi[1], Wei Tian[1]

[1]Department of Interventional Radiology, The First Affiliated Hospital of Nanjing Medical University, Nanjing, Jiangsu, China; [2]Department of Gerontology, The First Affiliated Hospital of Nanjing Medical University, Nanjing, Jiangsu, China

Received April 28, 2022; Accepted August 18, 2022; Epub October 15, 2022; Published October 30, 2022

Abstract: Objectives: Ferroptosis, a programmed cell death, has been recognized recently. Several studies have shown the connection between ferroptosis and biological processes in cancer. However, the potential role and mechanism of ferroptosis-related genes in hepatocellular carcinoma (HCC) remain unclear, and understanding the crosstalk between the tumor immune microenvironment and ferroptosis is still a great challenge. Method: We retrospectively analyzed the transcriptomic and clinical data of HCC from TCGA database. 74 ferroptosis-related genes (FRGs), including 14 immune-ferroptosis-related genes (IFRGs), were identified with differential expression in tumor and normal tissues. Then, we screened and constructed a prognostic signature using survival analysis and the least absolute shrinkage and selection operator. Furthermore, we validated the performance of the signature for assessing survival prognosis and clinicopathological staging. In addition, we investigated the link between the prognostic features and tumor-infiltrating immune cells using CIBERSORT. Result: The results identified HRAS, MAPK3 and TFRC as prognostic IFRGs. The risk score was elevated when IFRGs were upregulated and patient outcomes worsened. In addition, the results show significant differences in tumor-infiltrating immune cells, especially immunosuppressive cells, including tumor-infiltrating macrophages cells and regulatory cells, implying that the expression of these three IFRGs may be an intrinsic barrier to strong ferritin-induced immune responses. Enrichment analysis revealed crosstalk between ferroptosis and tumor immunity. The effect of the risk score was validated in the ICGC cohort and the Human Protein Atlas database confirmed the high expression of IFRGs in tumor tissue. Conclusions: In our study, these IFRGs may provide some new ideas for the study of ferroptosis and the tumor immunity. These findings may also provide new strategies for treatment of HCC.

Keywords: Liver cancer, ferroptosis, tumor microenvironment, bioinformatics, prognosis, TCGA, immune-ferroptosis-related gene

Introduction

Hepatocellular carcinoma (HCC) is one of the most common types of liver cancer and ranks as the second leading cause of cancer death worldwide [1]. More than 900,000 people were estimated to suffer from HCC globally in 2020, and over 830,000 deaths occurred [2]. Although the hepatitis B vaccine and antiviral drugs seem to decrease the rate of HCC morbidity yearly, China is still a high-risk area for HCC, and it still accounts for over half of liver cancer deaths worldwide [2-4]. The treatment of HCC depends not only on the tumor stage but also on liver function. In the early stage, curative resection with chemotherapy represents the primary therapy, and for patients within the Milan criteria, liver transplantation remains the best treatment for HCC [5-7]. However, insidious signs lead to great difficulty in the diagnosis of early stage HCC, as HCC is usually advanced when diagnosed, and the overall prognosis remains poor. Immunotherapy and molecular-targeted therapy have been recognized as comprehensive treatment models for advanced HCC [7, 8]. Sorafenib is the first-line treatment for patients with advanced disease and is the only anticancer drug that

causes ferroptosis in HCC [9, 10]. These studies suggest that ferroptosis and the tumor biology of HCC are closely related. Stockwell's team proposed an iron-dependent programmed cell death pathway called ferroptosis [11]. On the one hand, the disruption of iron metabolism causes an increase in intracellular free iron, which causes the generation of reactive oxygen species, which then leads to destruction of membranes. On the other hand, both glutathione (GSH) depletion and glutathione peroxidase 4 (GPX4) decline prohibit peroxides from being metabolized normally, which eventually compromises the integrity of cell membranes [12, 13]. Numerous genes are already implicated in the onset and control of ferroptosis according to recent investigations. These findings reveal the plasticity of ferroptosis in tumors, including hepatocellular carcinoma [14-16]. In addition, the tumor immune microenvironment (TIME) is correlated with iron homeostasis and metabolism in vivo, and ferroptosis plays a crucial role in tumor immunity, which has been reported to regulate the interaction between immune cells and the tumor microenvironment [17, 18]. However, the exact molecular mechanism, specifically in HCC, has not been clearly elucidated.

Herein, we retrospectively analyzed the expression profiles of ferroptosis-related genes (FRGs) by bioinformatics using RNA sequencing data from The Cancer Genome Atlas (TCGA) database. Relevant genes were extracted from FerrDb and ImmPort databases and screened for immune-ferroptosis-related genes (IFRGs) to explore their prognostic value for HCC. In addition, we developed a novel survival risk model based on IFRGs to predict the prognosis. Gene set enrichment analysis (GSEA) and CIBERSORT were used to further evaluate differences in immune-related biological characteristics across risk groups, and correlations between immune risk groups and common inhibitory checkpoint molecules were analyzed. Finally, the prognostic signature was validated in the International Cancer Genome Consortium (ICGC) cohort, and the three IFRGs were validated by immunohistochemistry in the Human Protein Atlas (THPA). We hope that this research will contribute to a deeper understanding of the ferroptosis-related genes and the tumor immune microenvironment in HCC.

Materials and methods

Acquisition and preprocessing of data

Transcriptome profiles of gene expression quantitative RNA sequencing and clinical information were downloaded from TCGA, which contains 370 cases (normal samples, 50 cases; tumor samples, 320 cases) after omitting those with incomplete critical clinical information.

173 ferroptosis-related driver and suppressor genes with the confidence of "validated" were obtained from the FerrDb database [19] as the criteria for FRG selection, and the immune-related genes (IRG) were acquired from the ImmPort database [20] in our study.

Identification of significantly different FRGs between HCC and non-tumorous samples

We retrospectively analyzed these data mentioned above. Differentially expressed ferroptosis-related genes (DE-FRGs) in normal and tumor samples were identified by differentiation analysis using the "limma" R package Heatmap and volcano plots of FRGs were drawn by the pheatmap and ggplot2 packages. The threshold was set to satisfy both a false discovery rate (FDR) less than 0.05 and an absolute value of the log2 fold change more than 0.5.

Gene ontology (GO) and Kyoto encyclopedia of genes and genomes (KEGG) enrichment analysis

DE-FRGs were applied to GO and KEGG analyses to identify the affected biological processes signaling pathways by the "clusterProfiler" R package. In the process, significant enrichment was defined as satisfying both q-value < 0.05 and *p*-value < 0.05.

Development of the IFRG prognostic signature

The IFRGs are defined as genes that are both FRGs and IRGs. We identified 14 potential prognostic IFRGs through Kaplan-Meier analysis and univariate Cox analysis by using the "surv" and "coxph" functions. Intersecting the two sets of genes resulted in three IFRGs.

Subsequently, these three IFRGs were put into the least absolute shrinkage and selection

operator analysis for screening and calculation of risk score using the "glmnet" R package. The risk score was derived by the this formula, with $Coef_j$ standing for the coefficient and X_j for the expression levels of each IFRG, standardized by z-score.

$$RiskScore = \sum_{n=1}^{j} Coef_j * X_j$$

Then, patients were classified into high and low-risk groups based on the median risk score. The survival analysis was conducted to evaluate the performance of the risk score.

Correlation between the prognostic signature and clinicopathological features

We loaded the "ggpubr" R package to conduct the correlation between each risk score and clinicopathological traits. The Wilcoxon rank-sum test or the Kruskal-Wallis rank-sum test was used to determine the statistical significance.

Gene set enrichment analysis

The Molecular Signatures Database was used to get the C2. CP. KEGG.v7.2 gene sets and Hallmark collections, and then the "clusterProfiler" R package was used to examine high- and low-risk populations to determine the functional differences between them.

Quantification of tumor-infiltrating immune cells (TIIC)

CIBERSORT provides 22 kinds of common infiltrating cell expression data as a reference which we used to assess the proportion of immune tissue cell distribution in all HCC cases [21]. The association between the risk score and immunological components was further supported.

Establishment of the nomogram

Risk scores and associated clinical characteristics were analyzed by multivariate Cox regression to determine independent predictors of patient survival. We used receiver operating characteristic (ROC) curves to assess the performance of the risk score and relevant clinical characteristics. Next, a nomogram was created to predict the overall survival at 1, 3, and 5 years. Internal validation of the model was tested using bootstrap resamples and a graphical display of the calibration plot was made.

Validation in ICGC data and the human protein Atlas database

The data of mRNA expression and clinical characteristics were downloaded from the ICGC database (https://dcc.icgc.org/) in HCC patients for external validation.

$$RiskScore = 0.3016 \times HRAS + 0.1907 \times MAPK3 + 0.1738 \times TFRC$$

The risk scores were derived from the formulas above and their relationship with survival prognosis and tumor immune was also validated. The protein expression of healthy cells, organs, and malignancies can be found in the Human Protein Atlas project (https://www.proteinatlas.org/). The expression of three crucial genes in normal tissues and tumor tissues was compared using IHC on this database.

Statistical analysis

We completed all statistical analyses and graphical displays using R 4.0.5. Continuous variables for two groups were examined with the Mann-Whitney U test or the Student's t test. Differences in survival analysis were assessed with the log-rank test. Unless otherwise stated, $P < 0.05$ was considered statistically significant.

Results

Identification and enrichment analysis of DE-FRGs

As shown in **Figure 1**, a total of 74 DE-FRGs between 50 normal and 320 tumor samples were extracted using the 'limma' R package (Table S1). Among them, 15 genes were upregulated and 59 genes were downregulated. **Figure 2A** and **2B** display the heatmap and volcano plots, respectively.

GO analysis indicated that DE-FRGs were enriched in cellular response to oxidative stress, response to metal ion, mitochondrial outer membrane, ferrous iron binding and transferrin receptor activity in biological process, molecular function and cellular component (**Figure 2C**; Table S2). KEGG analysis of DE-FRGs mainly includes ferroptosis, mitophagy-animal, autophagy-animal, and chemical carcinogenesis - reactive oxygen species, etc. (**Figures 2D**, S1; Table S3). These results con-

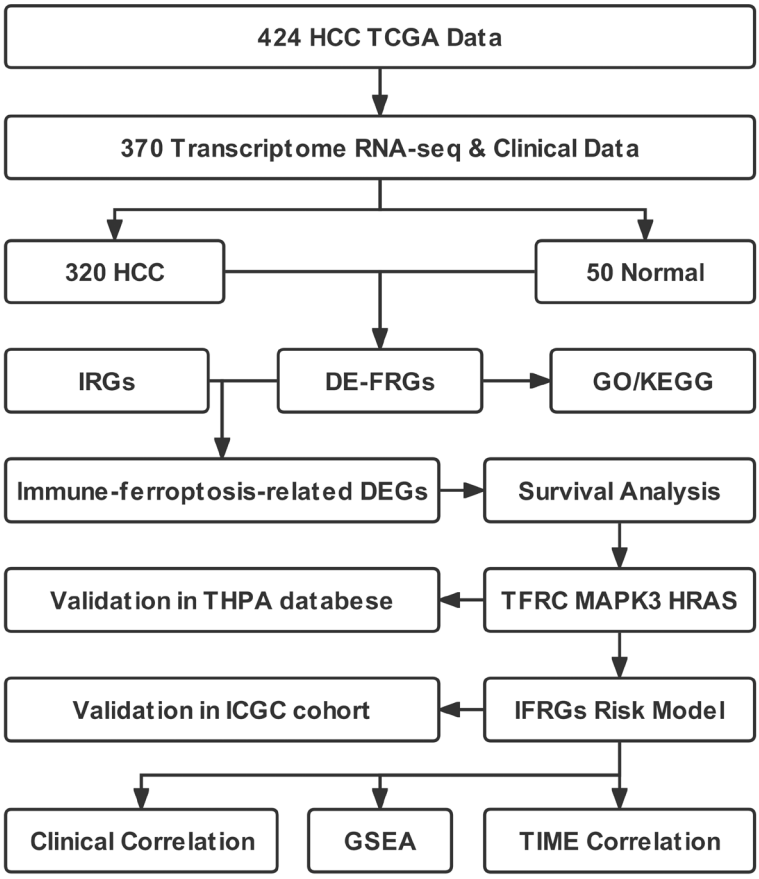

Figure 1. The flowchart of this study.

firmed that 74 DE-FRGs play an essential role in vital physiological processes and tumor development. Notably, some immune-related pathways were also enriched.

Construction of an IFRGs prognostic signature

To explore the function of the immune-related genes among DE-FRGs in disease, we first intersected the 74 DE-FRGs and the 1793 IRGs resulting in 14 IFRGs (**Figure 3A**), namely, BID, ELAVL1, HMOX1, HRAS, HSPA5, JUN, MAPK1, MAPK3, NRAS, PML, SRC, TFR2, TFRC, and TLR4 (Table S4).

The results of Cox regression and Kaplan-Meier analysis unexpectedly showed that three FRGs, including HRAS, MAPK1 and TFRC, were independent prognostic factors, and the survival was inversely correlated with the expression of these genes. This is contrary to our common belief that overexpression of ferroptosis-related gene is positively associated with prognosis in HCC (**Figure 3B-E**).

Therefore, we tried to design a prognostic signature by using these three IFRGs. A multivariate linear regression model was developed, which was able to evaluate the features of these three IFRGs. Three IFRG scores were chosen to create the risk score under penalized circumstances (lambda = 1): Risk score = (0.3016 × HRAS) + (0.1907 × MAPK3) + (0.1738 × TFRC).

Correlations between risk score and clinical information

After generating the risk score, we used survival analysis to detect the correlation between the risk score and survival. The outcome indicated that there was a negative correlation between risk score and survival (**Figure 4A**). The heatmap showed and compared the expression of three IFRGs (**Figure 4B**). The survival curves also suggested a poor probability of survival in the high-risk group than the low one (**Figure 4C**, **4D**).

Then, a further examination of the correlation between the risk score and clinical characteristics was performed (**Figure 4E-H**). The result suggested a significant escalation of risk scores as the stage and T-stage classification progressed (**Figure 4E**, **4F**, P = 0.0091, 0.013, 0.024, 0.039, respectively). These findings suggest that upregulation of IFRGs may contribute to a poor prognosis by promoting the progression and invasion of HCC.

Gene set enrichment analysis

The GSEA analysis also brought some results for the assessment of functional differences between the high- and low-risk groups. On the one hand, the high-risk score group genes for the C2 KEGG collection were primarily enriched in p53 signaling pathway, taking antigen processing and presentation, cancer and immune biological processes and toll-like receptor sig-

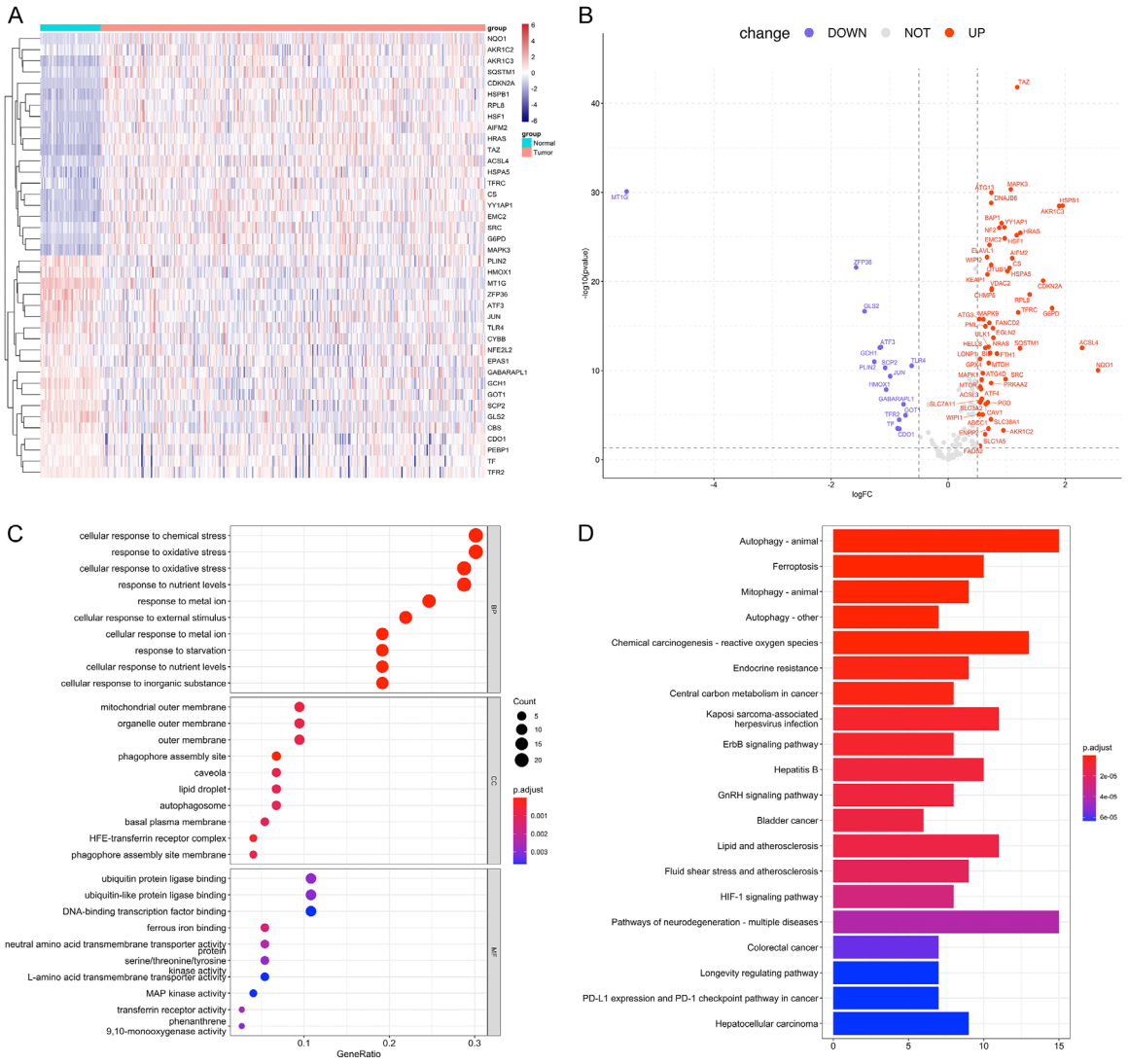

Figure 2. Volcano plot, heatmap, and enrichment analysis of Gene Ontology (GO) and Kyoto Encyclopedia of Genes and Genomes (KEGG) for Differentially expressed ferroptosis-related genes DE-FRGs. A. Heatmap for DE-FRGs generated by comparison of the tumor and normal tissues. The row name of the heatmap is the gene name, and the column name is the ID of samples not shown in the plot. B. Volcano plot for DE-FRGs. The purple and red dots represent the significantly downregulated and upregulated genes, respectively, and the gray dots represent the genes without differential expression. C, D. GO and KEGG enrichment analyses for DE-FRGs.

naling pathway as examples (**Figure 5A**; Table S5). Synchronously, the low-risk score cohort genes were mainly enriched in regulation-related and metabolism-related pathways, including fatty acid metabolism, complement and coagulation cascades and drug metabolism cytochrome p45 (**Figure 5B** and Table S5). Similarly, many immunological and metabolic processes were concentrated in the HALLMARK gene set (**Figure 5C**, **5D**; Table S5). The above results indicated that ferroptosis and immunity were closely related to molecular changes in the high- or low-risk group, and the risk score may be a viable predictor for various tumor microenvironment statuses in HCC.

Predicting tumor immune cell infiltration and common immune checkpoint expression by risk score

We then constructed immune cell profiles by CIBERSORT and analyzed the ratio of tumor-infiltrating immune subtypes to characterize the relationship between risk score and cell composition (**Figure 6A-C**). Then, the correlation analyses revealed that ten types of TIIC

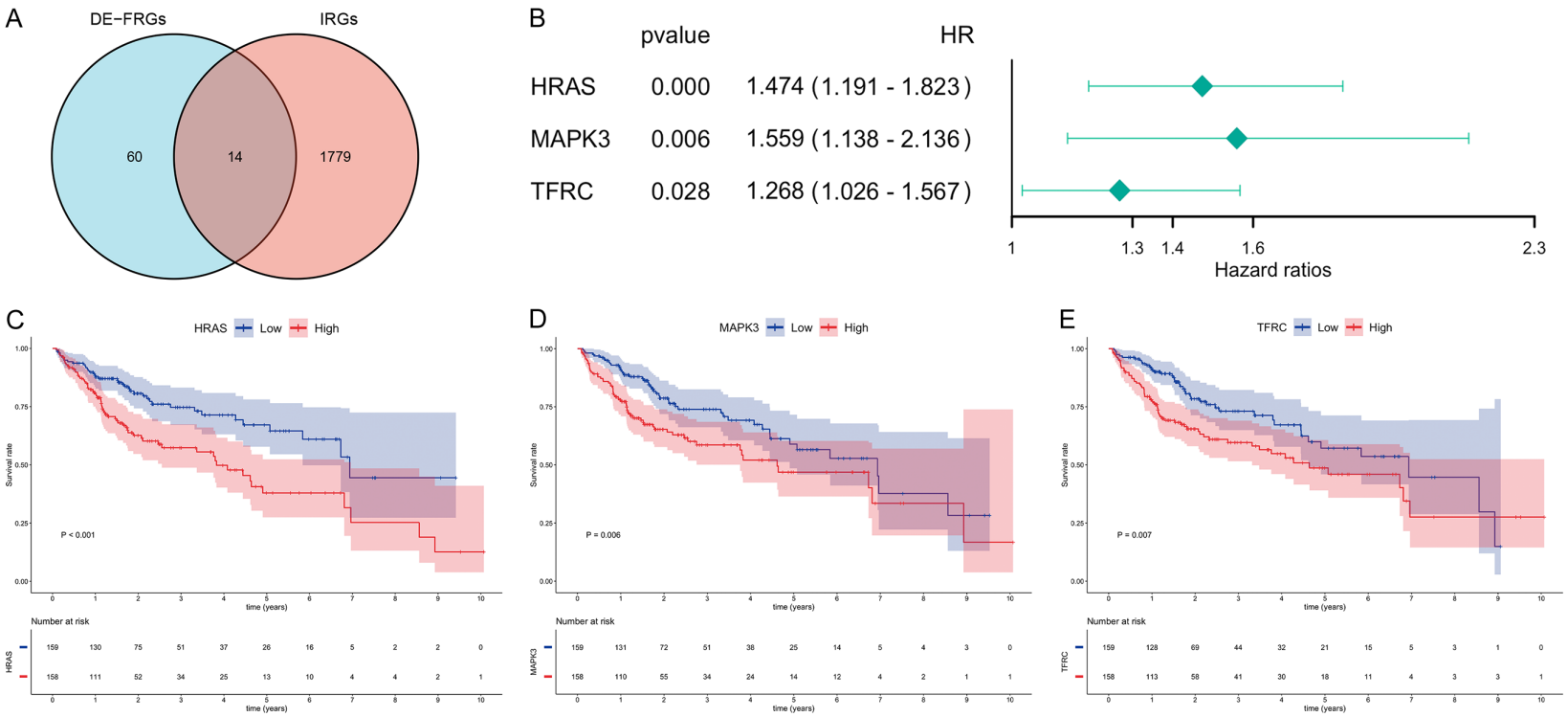

Figure 3. Find the immune-ferroptosis-related genes (IFRGs) in the TCGA cohort. A. A Venn diagram of DEGs. A comparison between 74 DE-FRGs and 1794 immune-related genes (IRGs), revealed 74 IFRGs. B. Prognostic analysis of 14 IFRGs using univariate Cox regression models. HRAS, MAPK3 and TFRC were found to be independent risk factors for HCC patients. C-E. Kaplan-Meier survival curves for patients with different expression levels of HRAS, MAPK3 and TFRC.

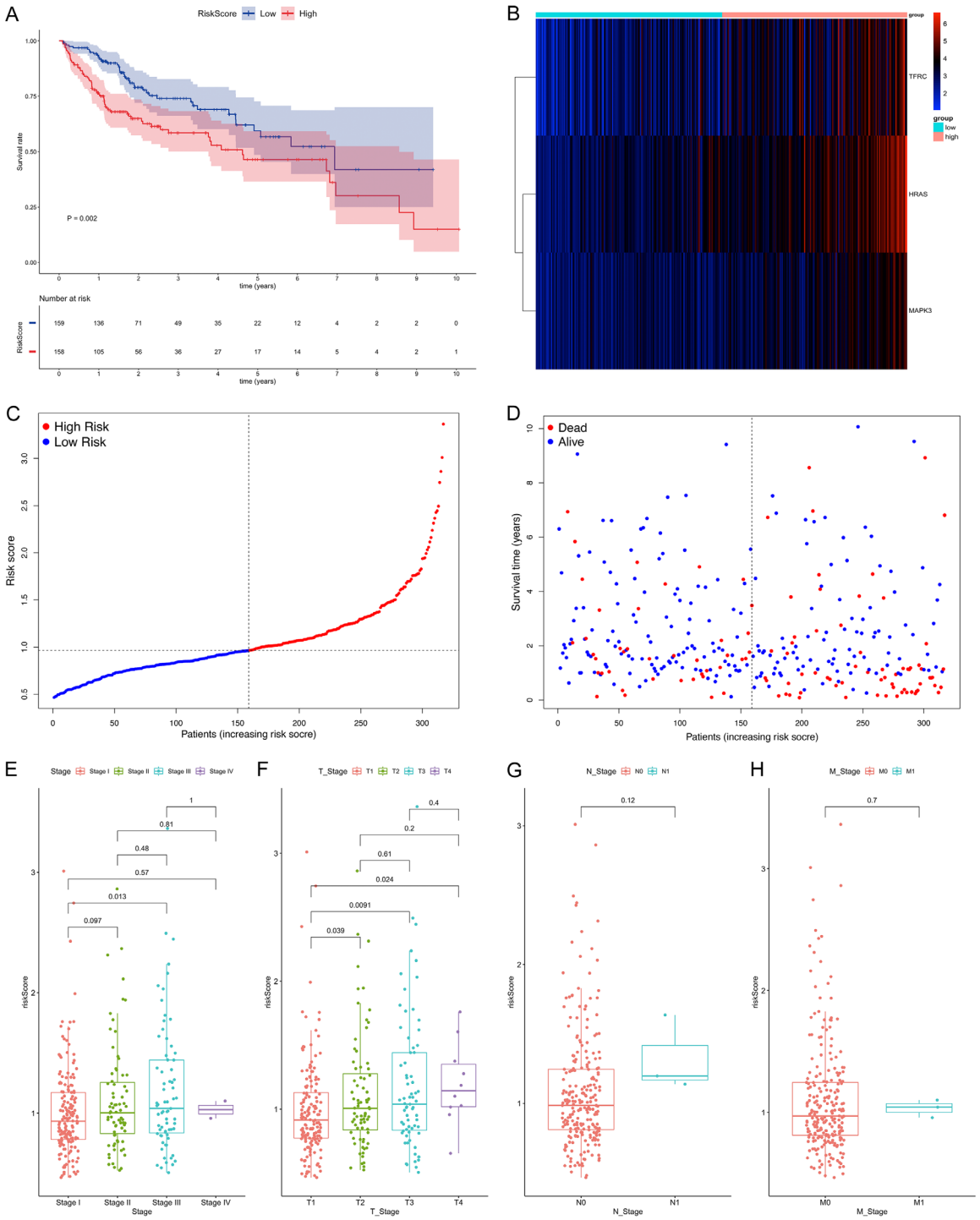

Figure 4. Validation of the IFRGs prognostic signature in the TCGA cohort. A. Kaplan-Meier survival curves for the high- and low-risk score groups. B. Heatmap of the expression of three IFRGs between the high- and low-risk groups. C. Risk score curve plot. The dashed line indicates the individual distribution of risk scores, and patients were divided into low-risk (blue) and high-risk (red) groups. D. Risk score scatter plot. Red dots indicate patients who died and blue dots indicate patients who are alive. As the risk score increases, more patients die. E-H. Relationship between risk score and clinicopathology, including stage, T stage, N stage, and M stage.

had a significant association with the risk score (**Figure 6D**; Table S6). The result showed a positive correlation between risk score and the four TIICs, including M0 macrophage, regulatory T cells (Tregs), follicular helper T cells and activated memory CD4 T cells; Six TIICs were nega-

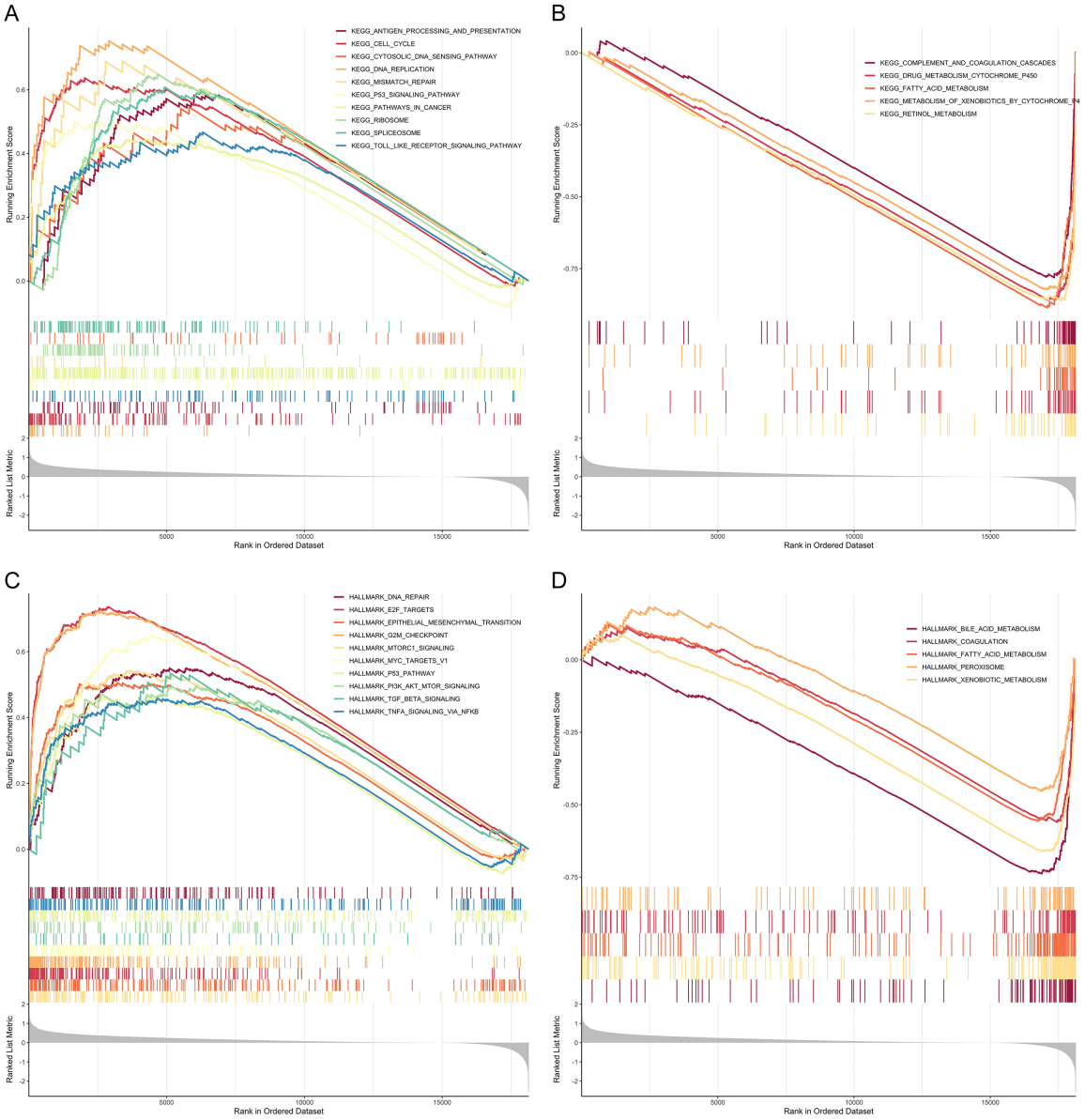

Figure 5. GSEA for samples in high- and low-risk score group. A, B. Enriched gene sets in the C2 collection, the KEGG gene sets, by samples in the high- and low-risk score groups. Each line represents one particular gene set with a unique color, and upregulated genes are located on the left, which approaches the origin of the coordinates; in contrast, the downregulated genes lie on the right of the x-axis. C, D. The enriched gene sets in the HALLMARK collection by samples in high- and low-risk score groups.

tively correlated with risk score, including M1 macrophages, resting memory CD4 T cells, resting mast cells, monocytes, resting NK cells and naive B cells. The results mentioned above further support the idea that the risk score can, in certain cases, serve as an immunological signal of HCC.

We also explored the correlation between risk score and common immune checkpoints (ICPs) to evaluate immunotherapy responses. A correlation was found between the risk score and ICPs revealing that the high-risk score group had high expression of ICPs (**Figure 6E**). The results revealed that patients with higher risk scores may showed a better response to immunotherapy.

Construction of the nomogram

It is necessary to look into the possibility that risk score may be an prognostic indicator. The

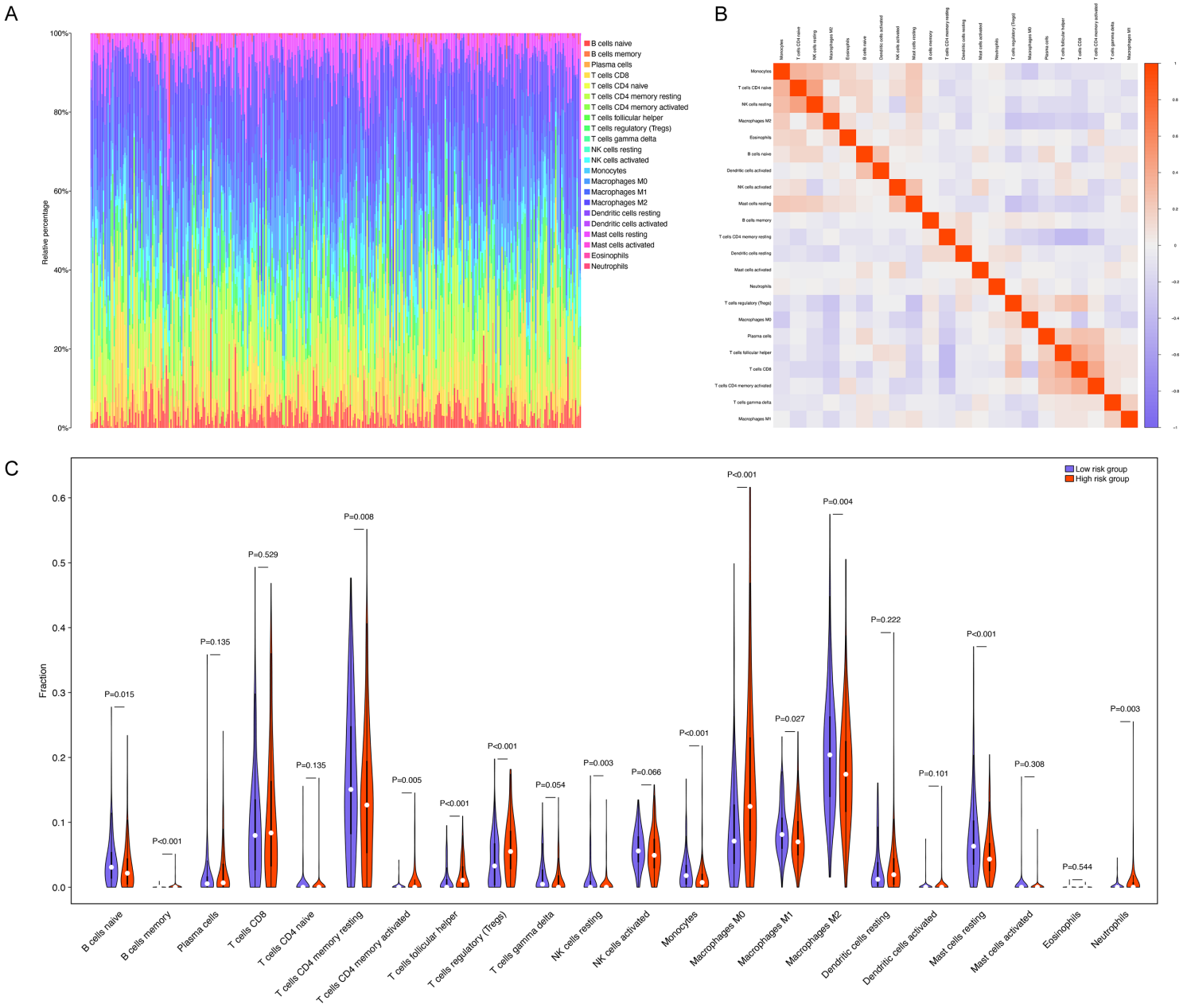
A
Relative percentage
100%
80%
60%
40%
20%
0%
B cells naive
B cells memory
Plasma cells
T cells CD8
T cells CD4 naive
T cells CD4 memory resting
T cells CD4 memory activated
T cells follicular helper
T cells regulatory (Tregs)
T cells gamma delta
NK cells resting
NK cells activated
Monocytes
Macrophages M0
Macrophages M1
Macrophages M2
Dendritic cells resting
Dendritic cells activated
Mast cells resting
Mast cells activated
Eosinophils
Neutrophils
B
C
Low risk group
High risk group
Fraction
P=0.015
P<0.001
P=0.135
P=0.529
P=0.135
P=0.008
P=0.005
P<0.001
P<0.001
P=0.054
P=0.003
P=0.066
P<0.001
P<0.001
P=0.027
P=0.004
P=0.222
P=0.101
P<0.001
P=0.308
P=0.544
P=0.003

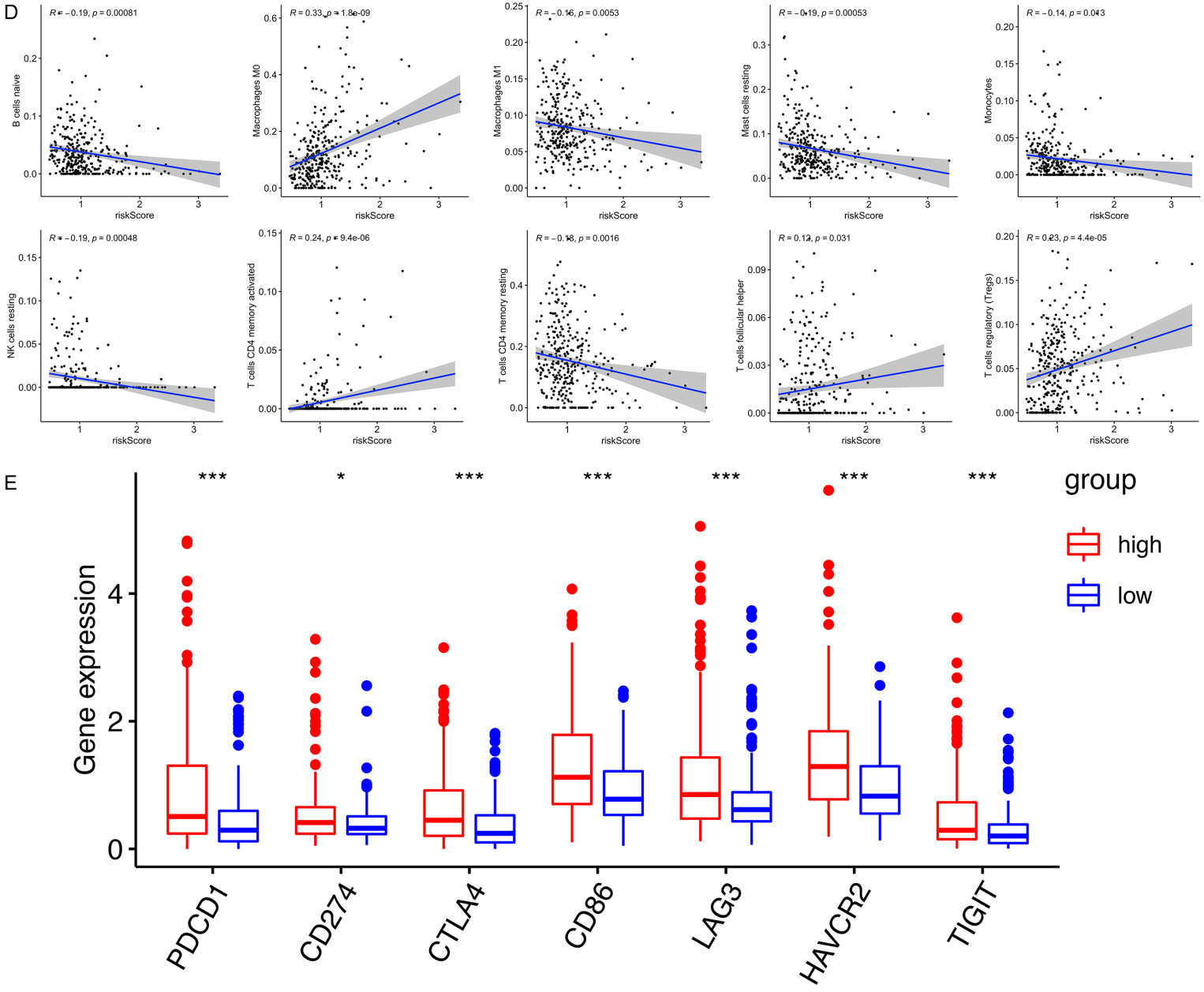
D
B cells naive
Macrophages M0
Macrophages M1
Mast cells resting
Monocytes
NK cells resting
T cells CD4 memory activated
T cells CD4 memory resting
T cells follicular helper
T cells regulatory (Tregs)
riskScore
E
Gene expression
group
high
low
PDCD1
CD274
CTLA4
CD86
LAG3
HAVCR2
TIGIT

Figure 6. Correlation of tumor-infiltrating immune cells and common ICPs with risk score. A. Bar plot shows the proportion of 22 types of tumor-infiltrating immune cells (TIICs) in TCGA tumor samples. The column names of the plot were sample ID. B. Heatmap showing the correlation between 22 kinds of TIICs and numeric numbers in each tiny box, indicating the *p*-value of the correlation between two cells. The shadow of each tiny color box represents a corresponding correlation value between two cells. C. Violin plot showing the ratio differentiation of 22 types of immune cells between the high- and low-risk groups. D. The scatter plot shows the correlation of the proportion of 10 kinds of TIICs with the risk score ($P < 0.05$). The blue line in each plot was a fitted linear model indicating the proportion tropism of the immune cell along with the risk score. E. The bar plot shows that the expression of ICPs was significantly higher in the high-risk score group than in the low-risk score group.

results showed that risk score and T stage were independent predictors of prognosis in patients (Table S7). In addition, we constructed a nomogram to predict survival time based on the above results (**Figure 7A**). The calibration curves suggested that the prognosis provided by the nomogram corresponded effectively to the actual fraction of survival (**Figure 7B-D**). Finally, the ROC curve showed a good predictive ability of our signature (**Figure 7E**, AUC = 0.659).

Validation of the IFRGs signature in the ICGC cohort

We derived risk score for HCC patients in the ICGC cohort using the same formula to verify whether the prognostic signature have similar predictive value in different cohorts. The heatmap of three hub genes in the ICGC cohort between the high- and low-risk groups is displayed in **Figure 8A**. Similarly, the survival analysis and survival curve also demonstrated that the high-risk group had lower overall survival than the low one (**Figure 8B-D**). In addition, **Figure 8E** and **8F** also show that the risk score can assess the altered immune microenvironment of the tumor to some extent.

Verifying the tissue expression level in the THPA database

To further validate the prognostic significance of the three genes, we obtained their transcription levels in healthy liver compared to HCC tissues in THPA. As **Figure 8G**, immunohistochemistry showed that the expression of HRAS, MAPK3 and TFRC were remarkably upregulated in HCC, which also supported our hypothesis.

Discussion

Approximately one million cases of hepatocellular carcinoma occur every year making it one of the most prevalent types of liver cancer, which causes a large financial, personal, and social burden to society [2]. Unfortunately, due to insidious progression, most patients are already in the middle-advanced stage when diagnosed with a poor prognosis. For these advanced patients, novel molecular targeted therapies and immunotherapies will be a step ahead of conventional therapies for a better prognosis, which has become one of the most exciting and promising developments in recent years [22-24]. Recent studies have shown that ferroptosis, a unique form of programmed cell death, plays a significant role in tumorigenesis and cancer treatment, especially in HCC. Sorafenib has been shown to specifically induce ferroptosis in cancer cells to achieve therapeutic effects [9, 25].

At present, many scholars have proven that there is considerable crosstalk between ferroptosis and immunity. On the one hand, ferroptosis induced by targeted therapy and immunotherapy may trigger the release of damage-associated molecular patterns (DAMPs), leading to the recruitment of dendritic cells with antigen capture and presentation and, finally, the induction of cytotoxic T cell responses. It has been reported that $CD8^+$ T cells induce ferroptosis in tumor cells in vivo, and this study obtained direct evidence of the connection between antitumor immunity and ferroptosis [18, 26]. On the other hand, ferroptosis in tumors may also impair the immune response. It has been shown that changes in the tumor immune microenvironment induced by ferroptosis will enhance tumor evasion of host immune surveillance instead, which may contribute to its development [27]. The complex relationship between ferroptosis-related pathways and genes in different aspects of immune function remains to be further explored.

In this research, we obtained gene expression data from the TCGA database. Differential analysis of ferroptosis-related genes identified 74 FRGs that were differentially expressed in

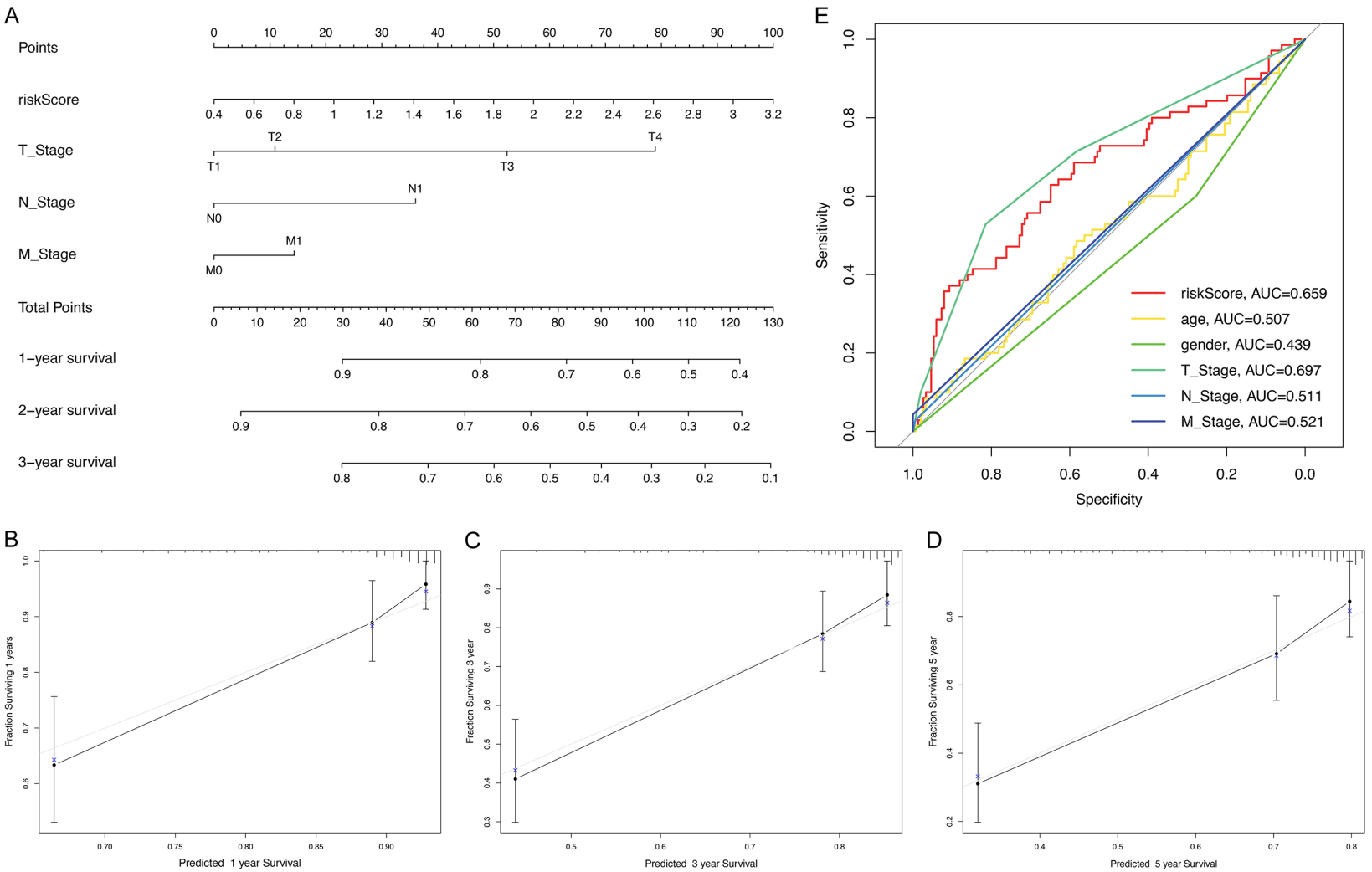

Figure 7. Establishment and validation of the nomogram. A. Establishment of a signature-based prognostic nomogram. B-D. Calibration curves of the nomogram prediction of 1-year, 3-year, and 5-year OS. E. ROC curve of the risk score and other relevant clinical parameters.

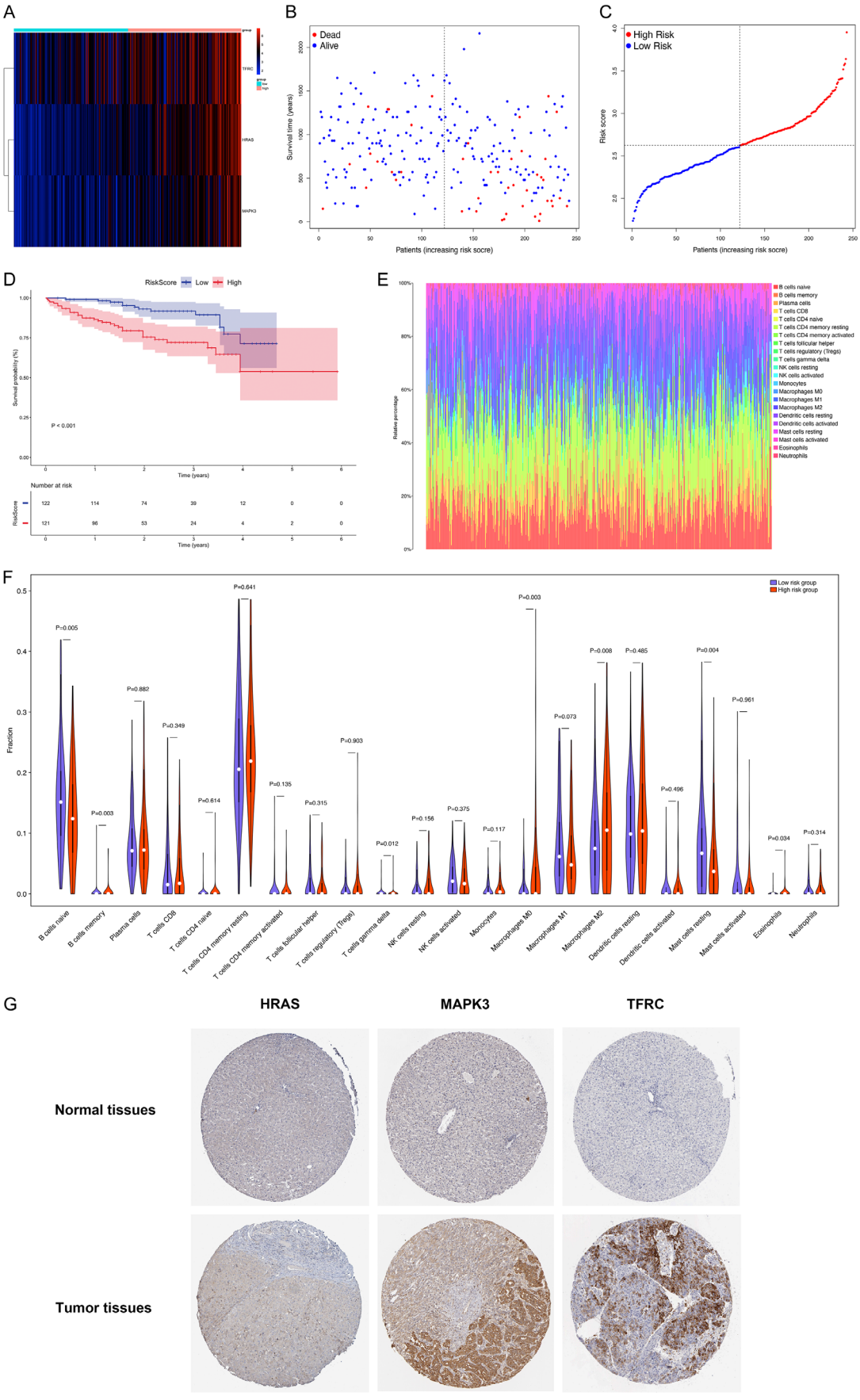
A
B
C
Dead
Alive
Survival time (years)
Patients (increasing risk socre)
High Risk
Low Risk
Risk score
Patients (increasing risk socre)
D
RiskScore
Low
High
Survival probability (%)
P < 0.001
Time (years)
Number at risk
E
Relative percentage
B cells naive
B cells memory
Plasma cells
T cells CD8
T cells CD4 naive
T cells CD4 memory resting
T cells CD4 memory activated
T cells follicular helper
T cells regulatory (Tregs)
T cells gamma delta
NK cells resting
NK cells activated
Monocytes
Macrophages M0
Macrophages M1
Macrophages M2
Dendritic cells resting
Dendritic cells activated
Mast cells resting
Mast cells activated
Eosinophils
Neutrophils
F
Low risk group
High risk group
Fraction
P=0.005
P=0.003
P=0.882
P=0.349
P=0.614
P=0.641
P=0.135
P=0.315
P=0.903
P=0.012
P=0.156
P=0.375
P=0.117
P=0.003
P=0.073
P=0.008
P=0.485
P=0.496
P=0.004
P=0.961
P=0.034
P=0.314
G
HRAS
MAPK3
TFRC
Normal tissues
Tumor tissues

Figure 8. Validation of the prognostic signature and gene expression in the International Cancer Genome Consortium (ICGC) cohort and the Human Protein Atlas (THPA) database. A. Heatmap of hub IFRGs expression between the high- and low-risk score groups in the ICGC cohort. B. Risk score scatter plot. C. Risk score curve plot. D. Kaplan-Meier survival curve. E, F. Bar plot of the proportion of 22 types of TIICs in ICGC tumor tissues. A violin plot shows the ratio and differentiation of 22 types of immune cells between the high- and low-risk groups. G. IHC of HRAS, MAPK3 and TFRC in HCC and normal tissues from the THPA database.

tumor and normal tissues. The enrichment analysis suggested that ferroptosis-related pathways and cancer-related pathways were significantly enriched, and we found that immune-related pathways were also indicated in the results. To further analyze the crosstalk of DE-FRGs in immunity, we identified the intersection of these DE-FRGs with IRGs. Survival analysis and Cox univariate regression analysis demonstrated the prognostic value of HRAS, MAPK3 and TFRC among these IFRGs. Surprisingly, the results showed that patients had a worse prognosis when these three IFRGs were upregulated, and we speculate that this might be due to the upregulation of the IFRGs leading to the immune suppressive pattern, which enhances cancer evasion of host antitumor immunity. Therefore, we used these three IFRGs to construct a signature for assessing prognosis and the tumor microenvironment. The results demonstrated that the risk score was strongly and inversely associated with prognosis and correlated with the tumor's pathological stage. In addition, we investigated the connection between the risk score and immune cells using CIBERSORT. We found significant differences in tumor immune infiltration, especially in immunosuppressive cells, including tumor-infiltrating macrophages and Treg cells, which implies that the expression of these three IFRGs may be an intrinsic barrier to the induction of strong immune responses by ferroptosis. In addition, GSEA also suggested an intimate association between the risk score and immune pathways. A nomogram was also developed integrating clinical characteristics and risk scores, and the ROC curves and calibration plots confirmed its prognostic accuracy. Finally, in the ICGC cohort, our prognostic signature is nicely suggestive of the prognostic and immune microenvironment of HCC, and we also found the expression of the hub genes was upregulated in tumor compared with normal tissues using the THPA database.

In HCC, the HRAS and MAPK3-mediated Ras/MAPK pathways play an important role in controlling major cytological processes such as cell proliferation, and their dysregulation is implicated in malignant transformation and progression [28]. HRAS is a common oncogene that belongs upstream of the Ras/MAPK signaling pathway and is responsible for transmitting extracellular signals to the nucleus to induce cell growth, division, maturation, and differentiation [29]. HRAS activating mutations are thought to be one of the main molecular mechanisms leading to activation of the MEK/ERK signaling pathway in chemically induced liver tumors in mice [30]. MAPK3, also known as extracellular regulatory protein kinase 1 (ERK1), belongs downstream of the Raf/MEK/ERK pathway, regulates cell proliferation, differentiation and survival, and plays a role in amplifying signals during tumor invasion and metastasis [31]. MAPK3 expression and activation were increased in human and animal hepatocellular carcinomas [32, 33]. Transferrin receptor, encoded by TFRC, is a membrane glycoprotein that can import iron by binding to plasma glycoprotein transferrin [34]. The significant increase in TFRC expression in human HCC cells and human HCC tissue samples and may be partially attributed to a posttranscriptional mechanism mediated by miR-152 downregulation [35].

HRAS, MAPK3 and TFRC are involved in the regulation of ferroptosis and tumor immunity. HRAS promotes the production of intracellular reactive oxygen species (ROS) during ferroptosis [36]. Ras/MAPK pathway activation and oncogenic RAS expression make cells more susceptible to inducers of ferroptosis [37-39]. However, overexpression of oncogenic HRAS has also been shown to be resistant to ferroptosis in tumors [40]. Regarding MAPK3, it has been reported that the phosphorylation status of MAPK3 is associated with tumor sensitivity to erastin, suggesting a correlation between its signaling and ferroptosis [39]. However, at the same time, MAPK3 is involved in the PI3K/AKT pathway and inhibits ferroptosis in cancer cells through SREBP1/SCD1-mediated adipogenesis

[41]. It has also been demonstrated that RAF-MEK1/2-ERK1/2 inhibitors inhibit the infiltration of regulatory T cells and monocytes/macrophages [31]. Therefore, HRAS and MAPK3, which are involved in the Ras/MAPK pathway, may show synergy in promoting ferroptosis, but their inhibition of antitumor immunity may inhibit the effect of ferroptosis to some extent. TFRC, which is involved in tumor progression, is abundantly expressed in hepatocellular carcinoma, and the accumulation of intracellular Fe^{2+} facilitates the development of ferroptosis in tumor cells [42]. However, HCC cell-imposed iron restriction results in reduced ferrous iron in TAMs and therefore drives their M2 polarization, which leads to suppression of tumor immunity [43]. Therefore, inducing TFRC upregulation leading to intracellular iron overload while inhibiting M2 polarization in macrophages may become a promising pathway for enhancing ferroptosis.

Using a combination of bioinformatics analysis, we constructed a risk model based on HRAS, MAPK3 and TFRC, validated it as a powerful tool to predict prognosis for HCC, and innovatively explored the crosstalk between immunity and ferroptosis. Since the crosstalk between immunity and ferroptosis in HCC has not been adequately studied, this study may also provide some ideas and directions that may contribute to new therapeutic approaches. In some aspects, our study also has some limitations. First, the clinical information downloaded from TCGA did not include patient treatment. Second, the interaction and mechanism of ferroptosis and tumor immunity are still unclear and more experiments are still needed to prove this hypothesis. Finally, the prognostic model needs to be validated in a real-world clinical cohort.

Conclusion

In conclusion, we identified higher expression levels of HRAS, MAPK3 and TFRC in HCC tumor tissues than in normal tissues. Prognostic signatures based on IFRGs are proposed to be of great value in predicting survival and reveal potential mechanisms of the immune process associated with the ferroptosis genes, which may become a promising therapeutic target for patients with HCC. Further studies are needed to validate these results in our research.

Acknowledgements

We are grateful to Zhouyue Wu (Key Laboratory of Cardiovascular & Cerebrovascular Medicine, School of Pharmacy, Nanjing Medical University) for her generous assistance in all stages of the present study. We acknowledge the TCGA database, ICGC database and The Human Protein Atlas for providing their platforms and contributors for uploading their meaningful datasets. We greatly appreciate the financial support from the National Natural Science Foundation of China (81901855), the Natural Science Foundation of Jiangsu Province (BK20181087), and the Jiangsu Planned Projects for Postdoctoral Research Funds (2020Z069).

Disclosure of conflict of interest

None.

Address correspondence to: Haibin Shi and Wei Tian, Department of Interventional Radiology, The First Affiliated Hospital of Nanjing Medical University, 300 Guangzhou Road, Nanjing 210029, Jiangsu, China. E-mail: shihb@njmu.edu.cn (HBS); tianwei@jsph.org.cn (WT)

References

[1] McGlynn KA, Petrick JL and El-Serag HB. Epidemiology of hepatocellular carcinoma. Hepatology 2021; 73 Suppl 1: 4-13.

[2] Sung H, Ferlay J, Siegel RL, Laversanne M, Soerjomataram I, Jemal A and Bray F. Global cancer statistics 2020: GLOBOCAN estimates of incidence and mortality worldwide for 36 cancers in 185 countries. CA Cancer J Clin 2021; 71: 209-249.

[3] Bray F, Ferlay J, Soerjomataram I, Siegel RL, Torre LA and Jemal A. Global cancer statistics 2018: GLOBOCAN estimates of incidence and mortality worldwide for 36 cancers in 185 countries. CA Cancer J Clin 2018; 68: 394-424.

[4] Chen W, Zheng R, Baade PD, Zhang S, Zeng H, Bray F, Jemal A, Yu XQ and He J. Cancer statistics in China, 2015. CA Cancer J Clin 2016; 66: 115-132.

[5] Clavien PA, Lesurtel M, Bossuyt PM, Gores GJ, Langer B and Perrier A; OLT for HCC Consensus Group. Recommendations for liver transplantation for hepatocellular carcinoma: an international consensus conference report. Lancet Oncol 2012; 13: e11-22.

[6] Pinna AD, Yang T, Mazzaferro V, De Carlis L, Zhou J, Roayaie S, Shen F, Sposito C, Cescon

M, Di Sandro S, Yi-Feng H, Johnson P and Cucchetti A. Liver transplantation and hepatic resection can achieve cure for hepatocellular carcinoma. Ann Surg 2018; 268: 868-875.
[7] Llovet JM, Kelley RK, Villanueva A, Singal AG, Pikarsky E, Roayaie S, Lencioni R, Koike K, Zucman-Rossi J and Finn RS. Hepatocellular carcinoma. Nat Rev Dis Primers 2021; 7: 1-28.
[8] Llovet JM, Ricci S, Mazzaferro V, Hilgard P, Gane E, Blanc JF, de Oliveira AC, Santoro A, Raoul JL, Forner A, Schwartz M, Porta C, Zeuzem S, Bolondi L, Greten TF, Galle PR, Seitz JF, Borbath I, Häussinger D, Giannaris T, Shan M, Moscovici M, Voliotis D and Bruix J; SHARP Investigators Study Group. Sorafenib in advanced hepatocellular carcinoma. N Engl J Med 2008; 359: 378-390.
[9] Chen S, Zhu JY, Zang X and Zhai YZ. The emerging role of ferroptosis in liver diseases. Front Cell Dev Biol 2021; 9: 801365.
[10] Lachaier E, Louandre C, Godin C, Saidak Z, Baert M, Diouf M, Chauffert B and Galmiche A. Sorafenib induces ferroptosis in human cancer cell lines originating from different solid tumors. Anticancer Res 2014; 34: 6417-6422.
[11] Dixon SJ, Lemberg KM, Lamprecht MR, Skouta R, Zaitsev EM, Gleason CE, Patel DN, Bauer AJ, Cantley AM, Yang WS, Morrison B and Stockwell BR. Ferroptosis: an iron-dependent form of nonapoptotic cell death. Cell 2012; 149: 1060-1072.
[12] Stockwell BR, Friedmann Angeli JP, Bayir H, Bush AI, Conrad M, Dixon SJ, Fulda S, Gascón S, Hatzios SK, Kagan VE, Noel K, Jiang X, Linkermann A, Murphy ME, Overholtzer M, Oyagi A, Pagnussat GC, Park J, Ran Q, Rosenfeld CS, Salnikow K, Tang D, Torti FM, Torti SV, Toyokuni S, Woerpel KA and Zhang DD. Ferroptosis: a regulated cell death nexus linking metabolism, redox biology, and disease. Cell 2017; 171: 273-285.
[13] Jiang X, Stockwell BR and Conrad M. Ferroptosis: mechanisms, biology and role in disease. Nat Rev Mol Cell Biol 2021; 22: 266-282.
[14] Yuan Y, Cao W, Zhou H, Qian H and Wang H. CLTRN, regulated by NRF1/RAN/DLD protein complex, enhances radiation sensitivity of hepatocellular carcinoma cells through ferroptosis pathway. Int J Radiat Oncol Biol Phys 2021; 110: 859-871.
[15] Jiang P, Yang F, Zou C, Bao T, Wu M, Yang D and Bu S. The construction and analysis of a ferroptosis-related gene prognostic signature for pancreatic cancer. Aging (Albany NY) 2021; 13: 10396-10414.
[16] Zhao L, Peng Y, He S, Li R, Wang Z, Huang J, Lei X, Li G and Ma Q. Apatinib induced ferroptosis by lipid peroxidation in gastric cancer. Gastric Cancer 2021; 24: 642-654.
[17] Stockwell BR and Jiang X. A physiological function for ferroptosis in tumor suppression by the immune system. Cell Metab 2019; 30: 14-15.
[18] Wang W, Green M, Choi JE, Gijón M, Kennedy PD, Johnson JK, Liao P, Lang X, Kryczek I, Sell A, Xia H, Zhou J, Li G, Li J, Li W, Wei S, Vatan L, Zhang H, Szeliga W, Gu W, Liu R, Lawrence TS, Lamb C, Tanno Y, Cieslik M, Stone E, Georgiou G, Chan TA, Chinnaiyan A and Zou W. CD8+ T cells regulate tumour ferroptosis during cancer immunotherapy. Nature 2019; 569: 270-274.
[19] Zhou N and Bao J. FerrDb: a manually curated resource for regulators and markers of ferroptosis and ferroptosis-disease associations. Database (Oxford) 2020; 2020: baaa021.
[20] Bhattacharya S, Andorf S, Gomes L, Dunn P, Schaefer H, Pontius J, Berger P, Desborough V, Smith T, Campbell J, Thomson E, Monteiro R, Guimaraes P, Walters B, Wiser J and Butte AJ. ImmPort: disseminating data to the public for the future of immunology. Immunol Res 2014; 58: 234-239.
[21] Newman AM, Liu CL, Green MR, Gentles AJ, Feng W, Xu Y, Hoang CD, Diehn M and Alizadeh AA. Robust enumeration of cell subsets from tissue expression profiles. Nat Methods 2015; 12: 453-457.
[22] Gotwals P, Cameron S, Cipolletta D, Cremasco V, Crystal A, Hewes B, Mueller B, Quaratino S, Sabatos-Peyton C, Petruzzelli L, Engelman JA and Dranoff G. Prospects for combining targeted and conventional cancer therapy with immunotherapy. Nat Rev Cancer 2017; 17: 286-301.
[23] Patel SA and Minn AJ. Combination cancer therapy with immune checkpoint blockade: mechanisms and strategies. Immunity 2018; 48: 417-433.
[24] Esteva FJ, Hubbard-Lucey VM, Tang J and Pusztai L. Immunotherapy and targeted therapy combinations in metastatic breast cancer. Lancet Oncol 2019; 20: e175-e186.
[25] Louandre C, Ezzoukhry Z, Godin C, Barbare JC, Mazière JC, Chauffert B and Galmiche A. Iron-dependent cell death of hepatocellular carcinoma cells exposed to sorafenib. Int J Cancer 2013; 133: 1732-1742.
[26] Efimova I, Catanzaro E, Van der Meeren L, Turubanova VD, Hammad H, Mishchenko TA, Vedunova MV, Fimognari C, Bachert C, Coppieters F, Lefever S, Skirtach AG, Krysko O and Krysko DV. Vaccination with early ferroptotic cancer cells induces efficient antitumor immunity. J Immunother Cancer 2020; 8: e001369.
[27] Yang WS, SriRamaratnam R, Welsch ME, Shimada K, Skouta R, Viswanathan VS, Cheah JH, Clemons PA, Shamji AF, Clish CB, Brown LM, Girotti AW, Cornish VW, Schreiber SL and Stockwell BR. Regulation of ferroptotic cancer cell death by GPX4. Cell 2014; 156: 317-331.

[28] Delire B and Stärkel P. The Ras/MAPK pathway and hepatocarcinoma: pathogenesis and therapeutic implications. Eur J Clin Invest 2015; 45: 609-623.
[29] Simanshu DK, Nissley DV and McCormick F. RAS proteins and their regulators in human disease. Cell 2017; 170: 17-33.
[30] Jaworski M, Buchmann A, Bauer P, Riess O and Schwarz M. B-raf and Ha-ras mutations in chemically induced mouse liver tumors. Oncogene 2005; 24: 1290-1295.
[31] Yang L, Zheng L, Chng WJ and Ding JL. Comprehensive analysis of ERK1/2 substrates for potential combination immunotherapies. Trends Pharmacol Sci 2019; 40: 897-910.
[32] Ito Y, Sasaki Y, Horimoto M, Wada S, Tanaka Y, Kasahara A, Ueki T, Hirano T, Yamamoto H, Fujimoto J, Okamoto E, Hayashi N and Hori M. Activation of mitogen-activated protein kinases/extracellular signal-regulated kinases in human hepatocellular carcinoma. Hepatology 1998; 27: 951-958.
[33] Huynh H, Nguyen TT, Chow KH, Tan PH, Soo KC and Tran E. Over-expression of the mitogen-activated protein kinase (MAPK) kinase (MEK)-MAPK in hepatocellular carcinoma: its role in tumor progression and apoptosis. BMC Gastroenterol 2003; 3: 19.
[34] Lopez A, Cacoub P, Macdougall IC and Peyrin-Biroulet L. Iron deficiency anaemia. Lancet 2016; 387: 907-916.
[35] Kindrat I, Tryndyak V, de Conti A, Shpyleva S, Mudalige TK, Kobets T, Erstenyuk AM, Beland FA and Pogribny IP. MicroRNA-152-mediated dysregulation of hepatic transferrin receptor 1 in liver carcinogenesis. Oncotarget 2016; 7: 1276-1287.
[36] Bartolacci C, Andreani C, El-Gammal Y and Scaglioni PP. Lipid metabolism regulates oxidative stress and ferroptosis in RAS-driven cancers: a perspective on cancer progression and therapy. Front Mol Biosci 2021; 8: 706650.
[37] Poursaitidis I, Wang X, Crighton T, Labuschagne C, Mason D, Cramer SL, Triplett K, Roy R, Pardo OE, Seckl MJ, Rowlinson SW, Stone E and Lamb RF. Oncogene-selective sensitivity to synchronous cell death following modulation of the amino acid nutrient cystine. Cell Rep 2017; 18: 2547-2556.
[38] Yang WS and Stockwell BR. Synthetic lethal screening identifies compounds activating iron-dependent, nonapoptotic cell death in oncogenic-RAS-harboring cancer cells. Chem Biol 2008; 15: 234-245.
[39] Yagoda N, von Rechenberg M, Zaganjor E, Bauer AJ, Yang WS, Fridman DJ, Wolpaw AJ, Smukste I, Peltier JM, Boniface JJ, Smith R, Lessnick SL, Sahasrabudhe S and Stockwell BR. RAS-RAF-MEK-dependent oxidative cell death involving voltage-dependent anion channels. Nature 2007; 447: 864-868.
[40] Schott C, Graab U, Cuvelier N, Hahn H and Fulda S. Oncogenic RAS mutants confer resistance of RMS13 rhabdomyosarcoma cells to oxidative stress-induced ferroptotic cell death. Front Oncol 2015; 5: 131.
[41] Yi J, Zhu J, Wu J, Thompson CB and Jiang X. Oncogenic activation of PI3K-AKT-mTOR signaling suppresses ferroptosis via SREBP-mediated lipogenesis. Proc Natl Acad Sci U S A 2020; 117: 31189-31197.
[42] Shen Y, Li X, Dong D, Zhang B, Xue Y and Shang P. Transferrin receptor 1 in cancer: a new sight for cancer therapy. Am J Cancer Res 2018; 8: 916-931.
[43] Sun JL, Zhang NP, Xu RC, Zhang GC, Liu ZY, Abuduwaili W, Wang F, Yu XN, Shi X, Song GQ, Wu H, Liu TT, Shen XZ, Deng B, Weng SQ, Dong L and Zhu JM. Tumor cell-imposed iron restriction drives immunosuppressive polarization of tumor-associated macrophages. J Transl Med 2021; 19: 347.

Table S1. Clinical characteristics of patients

	Alive	Dead	Overall
Number	213	107	320
Age (mean (SD))	58.66 (12.91)	60.29 (13.23)	59.21 (13.02)
Sex (%)			
male	157 (73.7)	64 (59.8)	221 (69.1)
female	56 (26.3)	43 (40.2)	99 (30.9)
OS (mean (SD))	2.73 (2.04)	1.82 (1.92)	2.43 (2.04)
Status (%)			
Alive	213 (100.0)	0 (0.0)	213 (66.6)
Dead	0 (0.0)	106 (99.1)	106 (33.1)
Not Reported	0 (0.0)	1 (0.9)	1 (0.3)
Stage (%)			
Stage I	124 (58.2)	37 (34.6)	161 (50.3)
Stage II	54 (25.4)	22 (20.6)	76 (23.8)
Stage III	35 (16.4)	45 (42.1)	80 (25.0)
Stage IV	0 (0.0)	3 (2.8)	3 (0.9)
T_Stage (%)			
T1	124 (58.2)	38 (35.5)	162 (50.6)
T2	55 (25.8)	22 (20.6)	77 (24.1)
T3	31 (14.6)	40 (37.4)	71 (22.2)
T4	3 (1.4)	7 (6.5)	10 (3.1)
N_Stage (%)			
N0	163 (76.5)	76 (71.0)	239 (74.7)
N1	1 (0.5)	2 (1.9)	3 (0.9)
NX	49 (23.0)	29 (27.1)	78 (24.4)
M_Stage (%)			
M0	167 (78.4)	76 (71.0)	243 (75.9)
M1	0 (0.0)	3 (2.8)	3 (0.9)
MX	46 (21.6)	28 (26.2)	74 (23.1)

Table S2. The result of GO enrichment analysis

ONTOLOGY	ID	Description	GeneRatio	BgRatio	*p*value	p.adjust	qvalue	Count
BP	GO:0062197	cellular response to chemical stress	22/73	360/18866	8.32E-21	1.33E-17	7.45E-18	22
BP	GO:0034599	cellular response to oxidative stress	21/73	310/18866	8.62E-21	1.33E-17	7.45E-18	21
BP	GO:0006979	response to oxidative stress	22/73	458/18866	1.48E-18	1.53E-15	8.52E-16	22
BP	GO:0031667	response to nutrient levels	21/73	473/18866	5.06E-17	3.92E-14	2.19E-14	21
BP	GO:0010038	response to metal ion	18/73	366/18866	2.08E-15	1.29E-12	7.19E-13	18
BP	GO:0071248	cellular response to metal ion	14/73	193/18866	1.86E-14	9.61E-12	5.37E-12	14
BP	GO:0042594	response to starvation	14/73	206/18866	4.61E-14	2.04E-11	1.14E-11	14
BP	GO:0071496	cellular response to external stimulus	16/73	326/18866	9.48E-14	3.67E-11	2.05E-11	16
BP	GO:0031669	cellular response to nutrient levels	14/73	221/18866	1.22E-13	3.77E-11	2.10E-11	14
BP	GO:0071241	cellular response to inorganic substance	14/73	221/18866	1.22E-13	3.77E-11	2.10E-11	14
BP	GO:0031668	cellular response to extracellular	14/73	253/18866	7.76E-13	2.18E-10	1.22E-10	14
BP	GO:0009267	cellular response to starvation	12/73	163/18866	1.34E-12	3.46E-10	1.93E-10	12
BP	GO:0071276	cellular response to cadmium ion	8/73	38/18866	1.51E-12	3.59E-10	2.01E-10	8
BP	GO:0046686	response to cadmium ion	9/73	64/18866	2.71E-12	6.00E-10	3.35E-10	9
BP	GO:0016236	macroautophagy	13/73	310/18866	1.77E-10	3.64E-08	2.04E-08	13
BP	GO:0070997	neuron death	13/73	360/18866	1.10E-09	2.13E-07	1.19E-07	13
BP	GO:0034614	cellular response to reactive oxygen species	9/73	170/18866	1.88E-08	3.41E-06	1.91E-06	9
BP	GO:0000302	response to reactive oxygen species	10/73	235/18866	2.32E-08	3.99E-06	2.23E-06	10
BP	GO:1901214	regulation of neuron death	11/73	321/18866	4.06E-08	6.61E-06	3.69E-06	11
BP	GO:0072584	caveolin-mediated endocytosis	4/73	12/18866	9.97E-08	1.54E-05	8.62E-06	4
CC	GO:0000407	phagophore assembly site	5/74	32/19559	1.26E-07	3.20E-05	2.09E-05	5
CC	GO:1990712	HFE-transferrin receptor complex	3/74	8/19559	2.87E-06	0.00036618	0.00023883	3
CC	GO:0005741	mitochondrial outer membrane	7/74	192/19559	8.13E-06	0.00069107	0.00045073	7
CC	GO:0005901	caveola	5/74	82/19559	1.47E-05	0.00083568	0.00054505	5
CC	GO:0031968	organelle outer membrane	7/74	218/19559	1.85E-05	0.00083568	0.00054505	7
CC	GO:0019867	outer membrane	7/74	220/19559	1.97E-05	0.00083568	0.00054505	7
CC	GO:0005811	lipid droplet	5/74	93/19559	2.71E-05	0.00089572	0.0005842	5
CC	GO:0034045	phagophore assembly site membrane	3/74	16/19559	2.81E-05	0.00089572	0.0005842	3
CC	GO:0005776	autophagosome	5/74	97/19559	3.32E-05	0.00094143	0.00061402	5
CC	GO:0009925	basal plasma membrane	4/74	51/19559	4.12E-05	0.0010514	0.00068574	4
CC	GO:0044853	plasma membrane raft	5/74	113/19559	6.91E-05	0.00160076	0.00104405	5
CC	GO:0005769	early endosome	8/74	377/19559	8.79E-05	0.00186875	0.00121883	8
CC	GO:0045178	basal part of cell	4/74	69/19559	0.00013549	0.00265768	0.00173339	4
CC	GO:0019898	extrinsic component of membrane	7/74	306/19559	0.00015727	0.00286447	0.00186826	7
CC	GO:0000792	heterochromatin	4/74	78/19559	0.00021789	0.00370418	0.00241593	4
CC	GO:0016323	basolateral plasma membrane	6/74	246/19559	0.00033773	0.0053517	0.00349048	6
CC	GO:0097413	Lewy body	2/74	8/19559	0.00038962	0.0053517	0.00349048	2
CC	GO:1990316	Atg1/ULK1 kinase complex	2/74	8/19559	0.00038962	0.0053517	0.00349048	2
CC	GO:0000421	autophagosome membrane	3/74	38/19559	0.00039875	0.0053517	0.00349048	3
CC	GO:0016605	PML body	4/74	102/19559	0.00060626	0.00718426	0.00468571	4
MF	GO:0008198	ferrous iron binding	4/74	26/18352	3.40E-06	0.00152168	0.00081342	4
MF	GO:0015175	neutral amino acid transmembrane transporter activity	4/74	34/18352	1.03E-05	0.00230328	0.00123124	4
MF	GO:0004998	transferrin receptor activity	2/74	2/18352	1.60E-05	0.00239	0.00127759	2

MF	GO:0031625	ubiquitin protein ligase binding	8/74	297/18352	2.56E-05	0.00285726	0.00152737	8
MF	GO:0004712	protein serine/threonine/tyrosine kinase activity	4/74	45/18352	3.20E-05	0.00286237	0.0015301	4
MF	GO:0044389	ubiquitin-like protein ligase binding	8/74	316/18352	3.97E-05	0.00296032	0.00158246	8
MF	GO:0018636	phenanthrene 9,10-monooxygenase activity	2/74	3/18352	4.80E-05	0.00306482	0.00163832	2
MF	GO:0004707	MAP kinase activity	3/74	20/18352	6.83E-05	0.00367263	0.00196323	3
MF	GO:0140297	DNA-binding transcription factor binding	8/74	347/18352	7.67E-05	0.00367263	0.00196323	8
MF	GO:0015179	L-amino acid transmembrane transporter activity	4/74	59/18352	9.37E-05	0.00367263	0.00196323	4
MF	GO:0047115	trans-1,2-dihydrobenzene-1,2-diol dehydrogenase activity	2/74	4/18352	9.57E-05	0.00367263	0.00196323	2
MF	GO:0061629	RNA polymerase II-specific DNA-binding transcription factor binding	7/74	267/18352	1.00E-04	0.00367263	0.00196323	7
MF	GO:0016655	oxidoreductase activity, acting on NAD(P)H, quinone or similar compound as acceptor	4/74	61/18352	0.00010681	0.00367263	0.00196323	4
MF	GO:0047086	ketosteroid monooxygenase activity	2/74	5/18352	0.00015915	0.00508135	0.00271628	2
MF	GO:0003725	double-stranded RNA binding	4/74	76/18352	0.00025089	0.00747642	0.00399658	4
MF	GO:0047023	androsterone dehydrogenase activity	2/74	7/18352	0.00033247	0.00883097	0.00472066	2
MF	GO:0015171	amino acid transmembrane transporter activity	4/74	82/18352	0.00033585	0.00883097	0.00472066	4
MF	GO:0051219	phosphoprotein binding	4/74	85/18352	0.00038527	0.00956761	0.00511444	4
MF	GO:0015186	L-glutamine transmembrane transporter activity	2/74	8/18352	0.00044213	0.01040167	0.0055603	2
MF	GO:0016705	oxidoreductase activity, acting on paired donors, with incorporation or reduction of molecular oxygen	5/74	162/18352	0.00049677	0.01110286	0.00593512	5

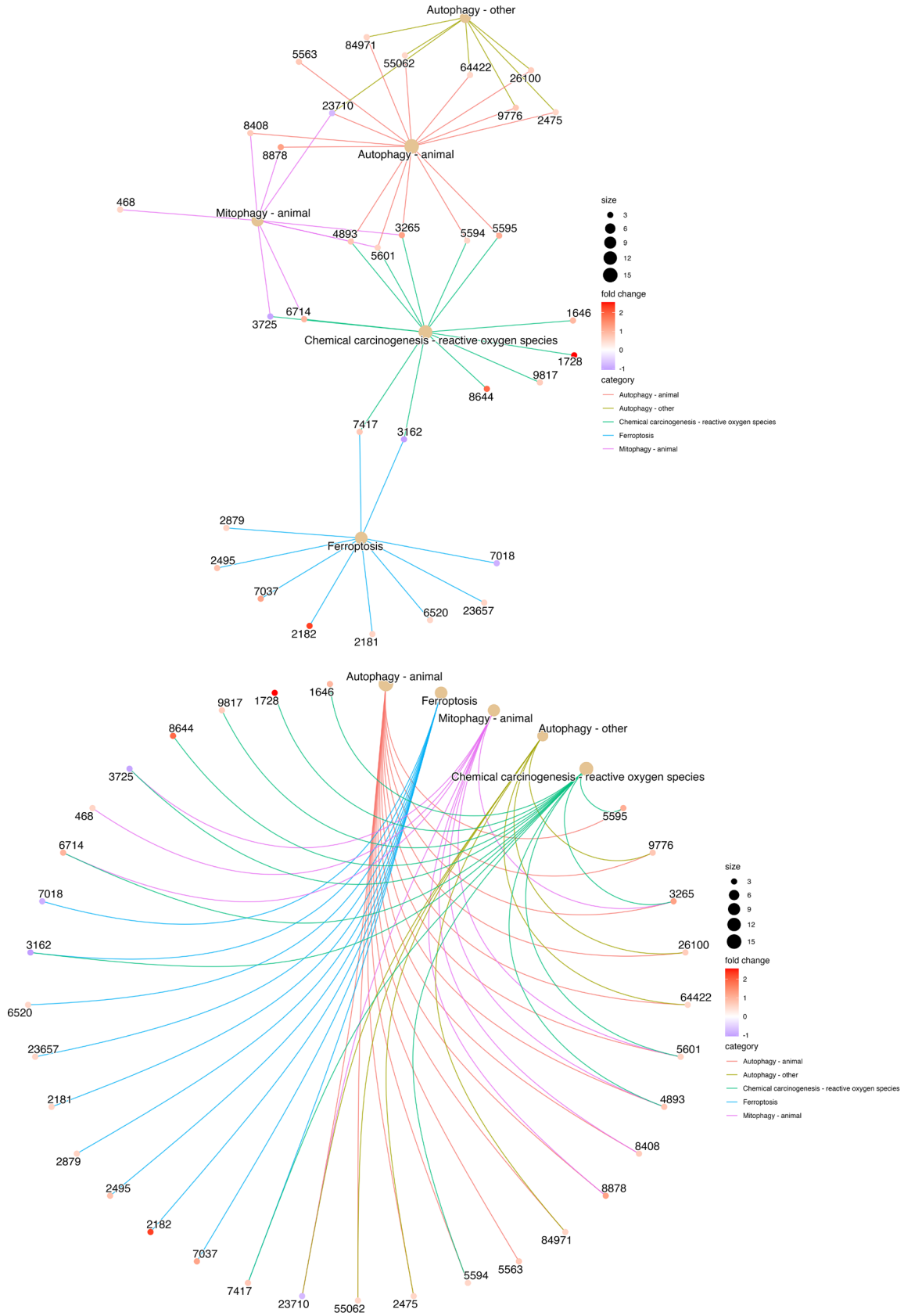

Figure S1. The cnetplot of the result of KEGG enrichment analysis.

Table S3. The result of KEGG enrichment analysis

ID	Description	GeneRatio	BgRatio	*p*value	p.adjust	qvalue	Count
hsa04140	Autophagy-animal	15/64	141/8112	1.45E-13	3.15E-11	1.18E-11	15
hsa04216	Ferroptosis	10/64	41/8112	4.16E-13	4.51E-11	1.69E-11	10
hsa04137	Mitophagy-animal	9/64	72/8112	3.82E-09	2.13E-07	7.94E-08	9
hsa04136	Autophagy-other	7/64	32/8112	3.92E-09	2.13E-07	7.94E-08	7
hsa05208	Chemical carcinogenesis-reactive oxygen species	13/64	223/8112	1.37E-08	5.96E-07	2.23E-07	13
hsa01522	Endocrine resistance	9/64	98/8112	6.01E-08	1.91E-06	7.12E-07	9
hsa05230	Central carbon metabolism in cancer	8/64	70/8112	6.15E-08	1.91E-06	7.12E-07	8
hsa05167	Kaposi sarcoma-associated herpesvirus infection	11/64	194/8112	2.71E-07	6.89E-06	2.57E-06	11
hsa04012	ErbB signaling pathway	8/64	85/8112	2.86E-07	6.89E-06	2.57E-06	8
hsa05161	Hepatitis B	10/64	162/8112	4.58E-07	9.93E-06	3.71E-06	10
hsa04912	GnRH signaling pathway	8/64	93/8112	5.76E-07	1.14E-05	4.24E-06	8
hsa05219	Bladder cancer	6/64	41/8112	6.88E-07	1.24E-05	4.65E-06	6
hsa05417	Lipid and atherosclerosis	11/64	215/8112	7.60E-07	1.27E-05	4.74E-06	11
hsa05418	Fluid shear stress and atherosclerosis	9/64	139/8112	1.22E-06	1.89E-05	7.04E-06	9
hsa04066	HIF-1 signaling pathway	8/64	109/8112	1.95E-06	2.81E-05	1.05E-05	8
hsa05022	Pathways of neurodegeneration-multiple diseases	15/64	476/8112	2.99E-06	4.05E-05	1.51E-05	15
hsa05210	Colorectal cancer	7/64	86/8112	4.48E-06	5.72E-05	2.14E-05	7
hsa04211	Longevity regulating pathway	7/64	89/8112	5.64E-06	6.36E-05	2.38E-05	7
hsa05235	PD-L1 expression and PD-1 checkpoint pathway in cancer	7/64	89/8112	5.64E-06	6.36E-05	2.38E-05	7
hsa05225	Hepatocellular carcinoma	9/64	168/8112	5.86E-06	6.36E-05	2.38E-05	9
hsa04370	VEGF signaling pathway	6/64	59/8112	6.17E-06	6.38E-05	2.38E-05	6
hsa04926	Relaxin signaling pathway	8/64	129/8112	6.90E-06	6.71E-05	2.50E-05	8
hsa05010	Alzheimer disease	13/64	384/8112	7.11E-06	6.71E-05	2.50E-05	13
hsa05166	Human T-cell leukemia virus 1 infection	10/64	222/8112	7.99E-06	7.23E-05	2.70E-05	10
hsa04210	Apoptosis	8/64	136/8112	1.02E-05	8.85E-05	3.31E-05	8
hsa05231	Choline metabolism in cancer	7/64	98/8112	1.07E-05	8.94E-05	3.34E-05	7
hsa05221	Acute myeloid leukemia	6/64	67/8112	1.30E-05	0.000105	3.91E-05	6
hsa05211	Renal cell carcinoma	6/64	69/8112	1.54E-05	0.000119	4.43E-05	6
hsa04625	C-type lectin receptor signaling pathway	7/64	104/8112	1.58E-05	0.000119	4.43E-05	7

Table S4. Results of 14 IFRGs obtained by intersecting with 74 DE-FRGs and 1793 IRGs

logFC	AveExpr	t	*P*.Value	adj.P.Val	B	change	logP	name
0.7157	3.298875	7.378368	1.07E-12	4.06E-12	18.01667	UP	11.97263	BID
0.704641	2.993683	11.0782	7.98E-25	9.12E-24	45.54489	UP	24.09791	ELAVL1
-1.059074	4.277569	-5.806083	1.38E-08	3.29E-08	8.772032	DOWN	7.860853	HMOX1
1.231322	3.488353	11.44838	3.49E-26	5.08E-25	48.64023	UP	25.45659	HRAS
1.01328	7.577856	10.25455	6.99E-22	5.33E-21	38.8465	UP	21.15558	HSPA5
-0.991007	5.094317	-6.413167	4.36E-10	1.29E-09	12.13392	DOWN	9.360909	JUN
0.547311	2.907179	5.932323	6.87E-09	1.74E-08	9.448541	UP	8.163286	MAPK1
1.068512	3.111673	12.74065	4.46E-31	3.57E-29	59.79926	UP	30.35097	MAPK3
0.771652	3.390913	7.963269	2.08E-14	9.53E-14	21.87852	UP	13.68101	NRAS
0.636289	1.829051	8.388239	1.05E-15	5.11E-15	24.81428	UP	14.97739	PML
0.980446	2.090715	6.282974	9.34E-10	2.72E-09	11.39011	UP	9.029603	SRC
-0.836812	6.773468	-4.203709	3.30E-05	5.93E-05	1.285612	DOWN	4.481967	TFR2
1.194979	3.100849	8.877083	3.00E-17	1.66E-16	28.31803	UP	16.52249	TFRC
-0.624357	1.175486	-6.859444	2.92E-11	9.33E-11	14.77486	DOWN	10.53508	TLR4

Table S5. The result of GSEA for samples in high- and low-risk score group

ID	setSize	enrichment	NES	*p*value	p.adjust	qvalues	rank
KEGG_DNA_REPLICATION	36	0.753949	1.968382	2.03E-07	1.86E-06	1.04E-06	2909
KEGG_CELL_CYCLE	124	0.637352	1.906124	1.00E-10	1.66E-09	9.28E-10	2030
KEGG_RIBOSOME	87	0.649174	1.898972	6.67E-09	8.14E-08	4.54E-08	4683
KEGG_ASTHMA	28	0.748842	1.886411	1.42E-05	8.99E-05	5.02E-05	2721
KEGG_PATHOGENIC_ESCHERICHIA_COLI_INFECTION	55	0.675147	1.870138	2.84E-07	2.36E-06	1.32E-06	3731
KEGG_SPLICEOSOME	125	0.608842	1.822976	6.40E-10	9.01E-09	5.03E-09	4931
KEGG_BLADDER_CANCER	41	0.648352	1.729311	0.0001	0.000483	0.00027	1866
KEGG_ANTIGEN_PROCESSING_AND_PRESENTATION	80	0.583648	1.696555	1.36E-05	8.92E-05	4.98E-05	6001
KEGG_LINOLEIC_ACID_METABOLISM	29	-0.815035	-2.703989	2.76E-08	2.97E-07	1.66E-07	805
KEGG_TYROSINE_METABOLISM	40	-0.795593	-2.840328	1.42E-10	2.16E-09	1.21E-09	984
KEGG_TRYPTOPHAN_METABOLISM	39	-0.8145	-2.849276	1.00E-10	1.66E-09	9.28E-10	931
KEGG_VALINE_LEUCINE_AND_ISOLEUCINE_DEGRADATION	43	-0.813644	-2.89901	1.00E-10	1.66E-09	9.28E-10	1053
KEGG_STEROID_HORMONE_BIOSYNTHESIS	55	-0.810303	-2.969803	1.00E-10	1.66E-09	9.28E-10	1216
KEGG_COMPLEMENT_AND_COAGULATION_CASCADES	69	-0.781048	-2.976624	1.00E-10	1.66E-09	9.28E-10	793
KEGG_METABOLISM_OF_XENOBIOTICS_BY_CYTOCHROME_P450	68	-0.822872	-3.147112	1.00E-10	1.66E-09	9.28E-10	1014
KEGG_FATTY_ACID_METABOLISM	42	-0.886223	-3.157011	1.00E-10	1.66E-09	9.28E-10	1051
KEGG_DRUG_METABOLISM_CYTOCHROME_P450	70	-0.860421	-3.281346	1.00E-10	1.66E-09	9.28E-10	1014
KEGG_RETINOL_METABOLISM	64	-0.862347	-3.285328	1.00E-10	1.66E-09	9.28E-10	511
HALLMARK_E2F_TARGETS	195	0.735993	2.266927	1.00E-10	6.25E-10	2.89E-10	2892
HALLMARK_G2M_CHECKPOINT	189	0.72179	2.219648	1.00E-10	6.25E-10	2.89E-10	2526
HALLMARK_MYC_TARGETS_V1	194	0.650795	2.003889	1.00E-10	6.25E-10	2.89E-10	4469
HALLMARK_MITOTIC_SPINDLE	198	0.573668	1.766711	1.00E-10	6.25E-10	2.89E-10	4024
HALLMARK_MTORC1_SIGNALING	195	0.543426	1.673802	8.55E-09	4.75E-08	2.20E-08	3680
HALLMARK_DNA_REPAIR	147	0.550106	1.666733	7.96E-07	3.62E-06	1.68E-06	5713
HALLMARK_ALLOGRAFT_REJECTION	195	0.531191	1.636116	5.78E-08	2.89E-07	1.34E-07	5438
HALLMARK_EPITHELIAL_MESENCHYMAL_TRANSITION	197	0.50612	1.558267	3.88E-06	1.62E-05	7.49E-06	3204
HALLMARK_SPERMATOGENESIS	133	0.506712	1.529947	0.000175	0.000626	0.00029	4070
HALLMARK_MYC_TARGETS_V2	58	0.546821	1.521308	0.001709	0.004497	0.002083	4112
HALLMARK_ADIPOGENESIS	192	-0.331301	-1.41297	0.000395	0.001234	0.000572	1531
HALLMARK_PEROXISOME	104	-0.452756	-1.863068	1.82E-05	6.99E-05	3.24E-05	1272
HALLMARK_COAGULATION	138	-0.560436	-2.296101	1.00E-10	6.25E-10	2.89E-10	688
HALLMARK_FATTY_ACID_METABOLISM	155	-0.555922	-2.31371	1.00E-10	6.25E-10	2.89E-10	1417
HALLMARK_XENOBIOTIC_METABOLISM	196	-0.661799	-2.874354	1.00E-10	6.25E-10	2.89E-10	1187
HALLMARK_BILE_ACID_METABOLISM	112	-0.738413	-2.981836	1.00E-10	6.25E-10	2.89E-10	1254

Table S6. The result of the correlation of the proportion of 10 kinds of TIICs with the risk score

gene	cell	rho	pval
riskScore	B cells naive	-0.1862336	0.00081472
riskScore	B cells memory	0.095679725	0.08748885
riskScore	Plasma cells	0.041700183	0.45726386
riskScore	T cells CD8	0.050486771	0.36802724
riskScore	T cells CD4 naive	-0.10728241	0.05521856
riskScore	T cells CD4 memory resting	-0.17541158	0.0016325
riskScore	T cells CD4 memory activated	0.244836457	9.41E-06
riskScore	T cells follicular helper	0.120940286	0.03054698
riskScore	T cells regulatory (Tregs)	0.226336512	4.39E-05
riskScore	T cells gamma delta	-0.02278735	0.68467648
riskScore	NK cells resting	-0.19408155	0.0004803
riskScore	NK cells activated	-0.02496582	0.65637485
riskScore	Monocytes	-0.13900586	0.01281114
riskScore	Macrophages M0	0.328055876	1.82E-09
riskScore	Macrophages M1	-0.15566463	0.00525864
riskScore	Macrophages M2	-0.09176943	0.10128477
riskScore	Dendritic cells resting	0.036265426	0.51801409
riskScore	Dendritic cells activated	0.003428219	0.95129069
riskScore	Mast cells resting	-0.19270148	0.00052787
riskScore	Mast cells activated	-0.06127652	0.2744441
riskScore	Eosinophils	0.100410911	0.0728592
riskScore	Neutrophils	0.077831717	0.16484632

Table S7. Independent prognostic indicators obtained by multivariate Cox regression

	coef	exp(coef)	se(coef)	z	p
age	0.003029	1.003034	0.010208	0.297	0.766653
gender (male)	0.099926	1.105089	0.271426	0.368	0.712761
risk score	0.856884	2.355809	0.235489	3.639	0.000274
T_Stage (T2)	0.251329	1.285733	0.364933	0.689	0.491012
T_Stage (T3)	1.244897	3.472579	0.298022	4.177	2.95E-05
T_Stage (T4)	1.872744	6.506126	0.543428	3.446	0.000569
N_Stage (N1)	0.889596	2.434147	0.736795	1.207	0.227284
M_Stage (M1)	0.361347	1.435262	0.739249	0.489	0.624981